


Characteristics of Ordovician paleokarst inclusions and their implications for paleoenvironmental and geological history in Halahatang area of northern Tarim Basin

Zhang Qingyu^{1,2}  · Qin Fengrui² · Liang Bin² · Cao Jianwen^{1,2} · DanYong² · Li Jingrui² · Chen Lixin³

Accepted: 13 October 2016 / Published online: 25 October 2016
© Springer-Verlag Berlin Heidelberg 2016

Abstract The Halahatang area has become a key region for petroleum exploration in the Tarim Basin in recent years owing to its well-developed and extremely heterogeneous Ordovician paleokarst carbonatites. This study explores the geochemical characteristics of the paleokarstification products, various periods of paleokarstification, and paleoenvironmental conditions of the Ordovician carbonates in the Halahatang area. After careful analysis of the rock fabric, the stable carbon and oxygen isotopic composition of the calcites filling paleokarstic fissures were systematically examined, and experimental analysis on fluid inclusions was conducted. The $\delta^{18}\text{O}$ values were generally negative, ranging from -4.14 to -15.71‰ with an average value of -9.95‰ . These values reflect a paleokarstification environment changing from shallow burial to deep burial, the rocks of which were later affected by corrosion. The $\delta^{13}\text{C}$ (PDB) values range from 2.12 to 4.09‰ with an average value of 0.65‰ . This confirms the complexity of the paleokarstification and revealed four different paleoenvironmental conditions: a marine environment with syndiagenesis, weathered crust exposed to a

freshwater karst environment, a shallow-burial karst environment, and a deep-burial high-temperature environment. The homogenization temperature of the inclusions indicates the existence of four paleokarstification and calcite infilling periods: buried karstification during the late Hercynian, the Indosinian–Yanshanian, and the Himalayan and karstification by meteoric water during the Caledonian. The results of this study provide new evidence for the prediction and exploration of karst reservoirs.

Keywords Carbon and oxygen isotopes · Calcite inclusions · Paleoenvironment · Paleokarst · Ordovician · Tarim Basin

Introduction

Paleokarst carbonatite reservoirs are widely distributed in China. With expanding applications of new technologies and methods for petroleum exploration, numerous paleokarst reservoirs have been identified in the Tarim Basin (Wu et al. 2012; Zhang et al. 2004), Qaidam (Feng et al. 2013), Ordos (Xia et al. 2007), and in the Sichuan Basin (Zhang et al. 2011). These findings have led to the development of various medium- and large-scale oil and gas fields, such as the Tahe, Lunnan, Changqing, and Weiyuan. This indicates that the paleokarst carbonatite reservoirs in China have great exploration potential (Jin and Cai 2006); therefore, expanding research into paleokarst reservoirs is very important for marine oil and gas exploration (Jia and Cai 2004; Liu 2007; Su et al. 2010).

Secondary karst reservoirs, such as corrosion pores, caves, and fissures of the Tarim Basin, the biggest petroliferous basin in China (Wu et al. 2012), were formed by paleokarstification and provide significant reservoir spaces

✉ Qin Fengrui
qinfengrui@karst.ac.cn

Zhang Qingyu
zhangqingyu@karst.ac.cn

¹ School of Environmental Studies, China University of Geosciences, 430074 Wuhan, China

² Institute of Karst Geology, Chinese Academy of Geological Sciences/Karst Dynamics Laboratory, MLR & GZAR; CAGS, 541004 Guilin, China

³ Research Institute of Exploration and Development, Tarim Oilfield Company, Petro China, 841000 Korla, Xinjiang, China

for oil (Zhang et al. 2011; Wang and Al-Aasm 2002; Chen et al. 2007; Ni et al. 2009). Deep-burial karstic reservoirs are important for marine carbonatite oil and gas fields. These reservoirs have a long geological history of environmental change and are influenced by corrosion and infilling involving several types of fluids over a variety of periods and from various factors to form heterogeneous and complex structures (Li et al. 1996; Zhu et al. 2005). These structures create difficulties in predicting deeply buried paleokarst carbonatite reservoirs.

Previous studies on fluid inclusions have been applied mainly to research on mineral deposits. Marray (1957) discovered large oil and gas inclusions in self-formed quartz. From the late 1970s to the early 1980s, fluid inclusion analysis has been used widely as a research tool in petroleum geology and paleokarstic reservoirs (Roedder 1979; Pagel and Poty 1983; Haszeldine et al. 1984; Pagel et al. 1985; Burley et al. 1989), promoting worldwide research on paleokarst and diagenetic fluids.

Fluid inclusions reflect the temperature and pressure during the formation of minerals and the properties of the initial fluid. Homogenization temperature can be used to investigate the temperature of paleofluids and to predict the geotemperature and geothermal evolution histories of basins (Osborne and Haszeldine 1993; Huang et al. 2008). The salinity and composition of the inclusions can yield information on the properties and origins of mineralizing fluids in basins (Veizer et al. 1999; Munz 2001; Wen et al. 2014). Inclusion analysis also serves as an important tool for studying diagenetic periods and environments (Mafia 1986; Yan et al. 2005; Liu et al. 2012).

Halahatang oil field, a key exploration area in Tarim Basin, includes well-developed Ordovician paleokarst carbonatites. Scientists have conducted numerous studies on the geological evolution, seismic response, characteristics of oil and gas reservoirs, and mechanisms of karst development in this area (Ni et al. 2010; Zhang et al. 2012, 2014; Wang et al. 2013; Liu et al. 2014). Constrained by limited research methods, data, and knowledge, currently, only Wang et al. (2013) have conducted preliminary inclusion research on Ordovician oil reservoirs in the Halahatang area. In contrast, nearby areas, such as Tahe and Tazhong oil fields, have been studied extensively (e.g., He et al. 2010; Zhang et al. 2011; Li 2013; Liu et al. 2013). Based on the analysis of rock fabric, this study systematically analyzes the isotopic compositions of carbon and oxygen and conducts experimental analysis on fluid inclusions to understand the paleoenvironmental conditions of Ordovician carbonatite paleokarstification. The results of this study will provide geochemical evidence for the prediction and exploration of karst reservoirs.

Study area and methods

Study area

The Halahatang oil field is located on the Halahatang nose-like tectonic belt in the Ordovician anticline of the Lunnan low uplift, which is located in the central part of the northern Tarim uplift. It encompasses an area of about 4000 km², neighboring the Luntai low uplift to the south, the Northern Depression to the north, the Yingmaili low uplift to the west, and the Lunnan low uplift to the east. This field is a favorable area for oil and gas migration from low to high potential areas, which favors petroleum accumulation (Fig. 1). It contains four blocks—the Ha6, Xinken, Rewapu, and Qiman—which are key exploration blocks of the Tarim Oilfield Company of China National Petroleum Corporation (CNPC) for Ordovician carbonatites in northern Tarim Basin (Zhang et al. 2012).

The Ordovician strata denudates and pinches out from south to north, outcropping the upper Ordovician Sangtamu (O_{3s}), Lianglitage (O_{3l}), Tumuxiuke (O_{3t}), middle Ordovician Yijianfang (O_{2y}), and lower Ordovician Yingshan formations (Fig. 2), respectively. The areas north and south of the pinch-out line of the Sangtamu Formation are dominated by a weathered crust karst of the paleo-hill and the buried karst overlain by clastic rocks, respectively.

Previous studies have shown that similar to the Tahe oil field (Zhang et al. 2012; Liu et al. 2013), the Halahatang area experienced three periods of depositional hiatus: between the end of Yijianfang Formation deposition and the beginning of the Tumuxiuke Formation, between the end of the Lianglitage Formation and the beginning of the Sangtamu Formation, and between the end of the Sangtamu Formation and the beginning of the Silurian Formation (Fig. 2).

In the study area, the upper Ordovician Sangtamu Formation (O_{3s}) is composed mainly of mudstone. The Lianglitage Formation (O_{3l}) is composed mainly of marlstone and nodular limestone interbedded with calcarenite, which can be divided into the Liang first section (O_{3l}^1), Liang second section (O_{3l}^2), and Liang third section (O_{3l}^3) from top to bottom. The Tumuxiuke Formation (O_{3t}) is dominated by taupe sparry limestone and marlstone. The middle Ordovician Yijianfang Formation (O_{2y}) is composed mainly of taupe sparry calcarenite, bioclastic limestone, and oolitic limestone (Fig. 2a, b). The middle to lower Ordovician Yingshan Formation (O_{1-2y}) can be divided into four sections from top to bottom: middle Ordovician Tongying first and second sections (O_{1y}^{1+2}), which are composed of

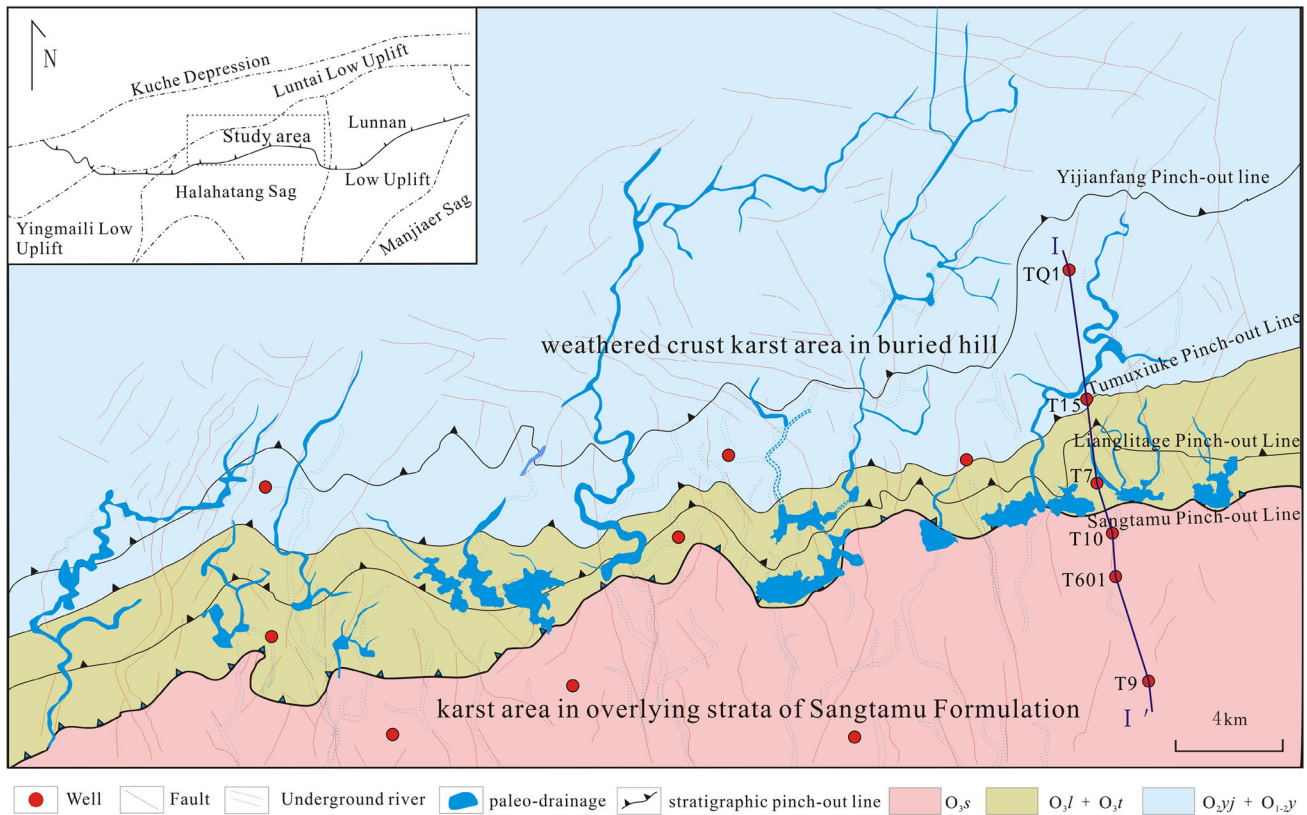
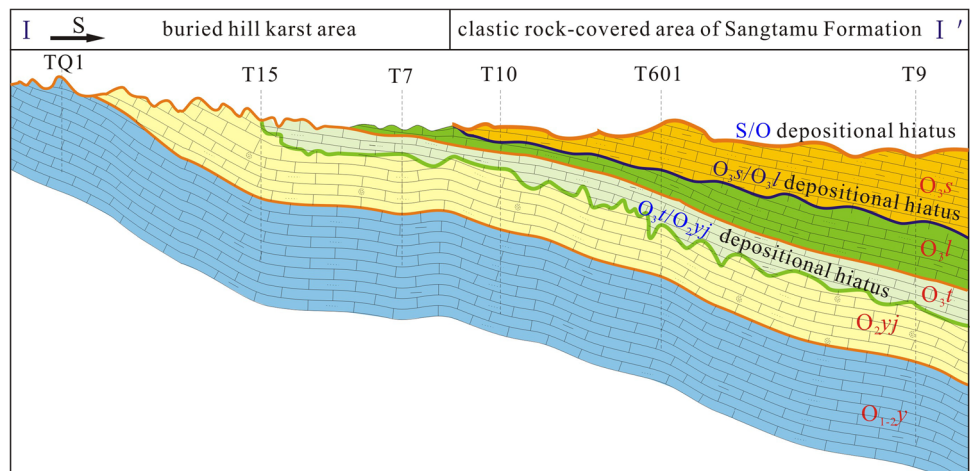


Fig. 1 Early Silurian geologic–tectonic background in the Halahatang area of northern Tarim Basin

Fig. 2 South–north-trending early Silurian geological section I–I' in the Halahatang area of northern Tarim Basin



thick gray micrite interbedded with sparry calcarenite, and lower Ordovician Tongying third and fourth sections (O_{1y}^{3+4}), which are composed of limestone interbedded with dolomitic limestone. The lower Ordovician Penglai Formation (O_{1p}) is composed mainly of dolomite, although few wells are drilled to this stratum. The Yijianfang and Yingshan formations consist of strongly developed karst strata and well-developed thick limestone and serve as the main reservoirs of oil and gas in this area (Fig. 3).

Samples and experiments

The samples were collected mainly from the carbonate strata of the Ordovician Yingshan (O_{1-2y}) and Yijianfang (O_{2yj}) formations in the Halahatang area. These samples include calcites filling karst fissures and pores of the Ordovician carbonates, which either partly or fully fill the fissures and holes of the paleokarst. The sampling depth ranged from 6685.8 to 6837.6 m, which is 0.5–155 m beneath the Ordovician paleo-weathered crust. From 10

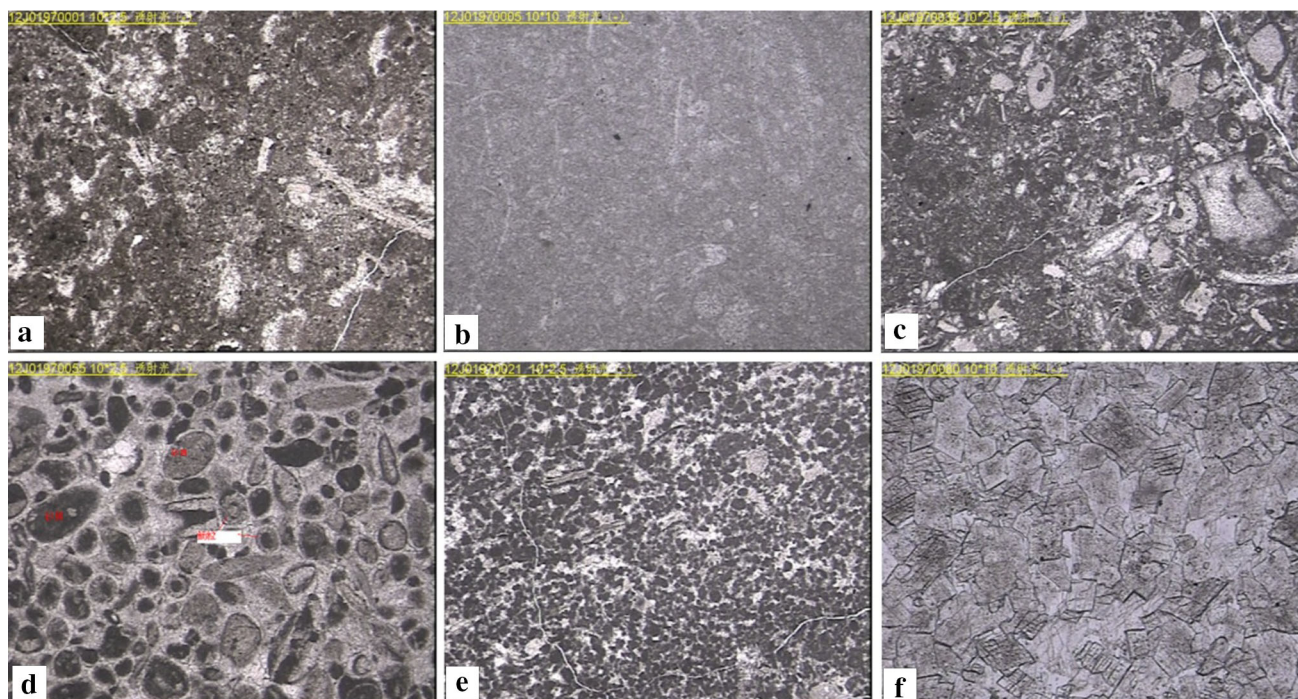


Fig. 3 Petrological characteristics of Ordovician carbonatite rocks from Halahatang. **a** Well T9, O_{3l} , microcrystalline silt bioclastic limestone, 10×2.5 light transmission (-), transverse diameter of the visual field 5.12 mm; **b** Well T601, O_{3t} , microcrystalline bioclastic limestone, 10×10 light transmission (-), transverse diameter of the visual field 1.27 mm; **c** Well T10, O_{2yj} , sparry bioclastic limestone, 10×2.5 light transmission (-), transverse diameter of the visual field

5.12 mm; **d** Well T7, O_{2yj} , sparry arenitic–oolitic limestone, 10×2.5 light transmission (-), transverse diameter of the visual field 5.12 mm; **e** Well T15, O_{1-2y} , sparry arenitic limestone, 10×2.5 light transmission (-), transverse diameter of the visual field 5.12 mm; **f** Well TQ1, O_{1p} , medium-grain dolostone, 10×2.5 light transmission (-), transverse diameter of the visual field 5.12 mm

wells, 32 samples were collected for carbon and oxygen isotopic analysis, including eight samples of infilling calcite from fissures and pores and four limestone samples. For analysis of inclusions, 15 samples were collected from which 350 calcite inclusions were examined using the THMSG600 Cooling–Heating Stage (Linkam Company, Britain). Analysis was conducted in the Zhongnan Supervision and Inspection Center of the Ministry of Land and Resources of the People’s Republic of China (MLR), which measures temperatures ranging from -190 to 600 °C and has a reproduction error <2 °C for the homogenization temperature and <0.2 °C for the freezing point.

In the inclusion tests, the temperature was increased at varying speeds. The heating rate was increased by 3 °C/min in the lower temperatures <31 °C but was decreased to 0.2 – 0.5 °C/min when the temperature was close to the initial melting point, freezing point, and clathrate melting temperature of CO_2 . The heating rate generally ranged from 10 to 15 °C/min at medium or high temperatures >31 °C but decreased to 1 °C/min near the phase change temperature. The salinity of the inclusions was calculated on the basis of the salinity–freezing point equation of the H_2O – $NaCl$ system (Lu and Shan 2015):

$$W = 1.78T - 0.0442T^2 + 0.000557T^3, \quad (1)$$

where W is the weight percentage of $NaCl$, and T is the decrease of the freezing point. The salinity of the H_2O – CO_2 – $NaCl$ three-phase inclusions was calculated on the basis of the temperature of clathrates:

$$W_{NaCl} = 15.52022 - 1102342T - 0105286T^2, \quad (2)$$

where W_{NaCl} is the mass fraction of $NaCl$ in the aqueous solution, and T is the clathrate melting temperature (Lu and Shan 2015).

Analysis of carbon and oxygen isotopes was conducted in the Supervision and Inspection Center on Karst Geological Resources and Environment at the MLR. The carbon isotopic values were analyzed online using the combined technology of Gasbench II and MAT253. Analytical accuracy was ensured by correction to the Chinese national carbonate standards (GBW04405, GBW04406, GBW04416, and GBW04417) and was monitored using the international standard calcite material (NBS18). The standard deviations of $\delta^{13}C$ and $\delta^{18}O$ were 0.005 and 0.07% , respectively. The results are expressed in terms of the Pee Dee Belemnite (PDB) standard. During analysis, the temperature and humidity were 25 °C and 60% , respectively.

Results and analysis

Geochemical characteristics of carbon and oxygen isotopes

The abundance of ^{13}C and ^{18}O in marine carbonates is affected mainly by sea-level change, the origin and burial rate of organic carbon, and the oxidation–reduction conditions of the sedimentation–diagenetic environment (Zheng and Chen 2000; Zhang et al. 2011). Therefore, the composition of carbon and oxygen isotopes in the carbonates varies with the sedimentation–diagenetic environment and the properties of diagenetic fluids. The carbon and oxygen isotopic results of the 32 calcite infillings of the Ordovician carbonatite from the Halahatang area are shown in Table 1.

The large number of results indicates that the isotopic values of modern marine inorganic carbonates are close to 0‰ for both $\delta^{13}\text{C}$ and $\delta^{18}\text{O}$ values (Liu et al. 2004; Gu 2000). However, the results indicate a broad range of $\delta^{13}\text{C}$ and $\delta^{18}\text{O}$ values of the fillings in the paleokarst fissures and pores of Ordovician carbonatite in the Halahatang area (Table 1). $\delta^{13}\text{C}$ varied from 2.12 to -4.09‰ with an average of -0.65‰ , and $\delta^{18}\text{O}$ varied from -4.14 to -15.71‰ with an average of -9.95‰ . In contrast, Gu (2000) reported that the average initial $\delta^{18}\text{O}$ value of marine carbonatite from Devonian to Cambrian ranges from -4 to -5‰ . Liu et al. (2008) found that the $\delta^{13}\text{C}$ value of microcrystalline limestone in the Tahe oil field ranges from -1.697 to 0.921‰ with an average of -0.45‰ and that the $\delta^{18}\text{O}$ value ranges from -8.64 to

-4.153‰ . Compared with these previous findings, the present results differ significantly with a considerably lower $\delta^{18}\text{O}$ value.

However, the results of the present study are similar to those reported for the western Lungu area, in which $\delta^{13}\text{C}$ ranges from -0.70 to -6.50‰ with an average of -1.76 and $\delta^{18}\text{O}$ ranges from -3.75 to -17.10‰ with an average of -9.42‰ (Liu et al. 2004). Moreover, the Tahe oil field average $\delta^{13}\text{C}$ is -0.807‰ , and the average $\delta^{18}\text{O}$ is -9.14‰ , as derived from the analysis of 21 data points (Liu et al. 2008). The present results differ slightly from those reported for the eastern Lungu area in which the average $\delta^{13}\text{C}$ is -1.40‰ and the average $\delta^{18}\text{O}$ is -10.74‰ , as derived from the analysis of 25 data points (Zhang et al. 2015). The results of the present study also differ from those reported for Well TZ12 in the central Tarim area in which the average $\delta^{13}\text{C}$ is -1.08‰ and the average $\delta^{18}\text{O}$ is -7.05‰ , as derived from the analysis of four sampling sites. Only a few sampling sites show the isotopic values drifting toward the two ends.

The isotopic characteristics of carbon and oxygen in the minerals filling pores and fissures reflect the isotopic abundance of secondary minerals. The $\delta^{13}\text{C}$ and $\delta^{18}\text{O}$ values of calcites showed significantly different distributions in this study. The $\delta^{18}\text{O}$ values were generally negative with an average of -9.95‰ , indicating a paleokarstification changing from shallow burial to deep burial and later effects of corrosion and filling. The $\delta^{13}\text{C}$ values can be either positive or negative, ranging from -1.697 to 0.921‰ , which verifies the complexity of paleokarstification.

Table 1 Carbon and oxygen isotopic compositions of the bedrock and calcites filling the karst fissures and pores

No.	Layer	Depth/m	Sample	$\delta^{13}\text{C}_{(\text{V-PDB})}\text{‰}$	$\delta^{18}\text{O}_{(\text{V-PDB})}\text{‰}$	No.	Layer	Depth/m	Sample	$\delta^{13}\text{C}_{(\text{V-PDB})}\text{‰}$	$\delta^{18}\text{O}_{(\text{V-PDB})}\text{‰}$
1	O _{2y}	6756.1	Calcite	-3.79	-15.17	17	O _{2y}	6710.6	Calcite	-0.32	-13.51
2	O _{2y}	6756.6	Calcite	-0.47	-11.74	18	O _{1-2y}	6824.3	Calcite	-1.35	-14.26
3	O _{1-2y}	6733.1	Calcite	-3.44	-13.13	19	O _{2y}	6743.2	Calcite	0.34	-13.92
4	O _{1-2y}	6725.5	Calcite	-3.81	-11.92	20	O _{1-2y}	6837.6	Calcite	1.98	-4.510
5	O _{1-2y}	6709.2	Calcite	1.16	-5.80	21	O _{2y}	6788.6	Calcite	-3.12	-10.25
6	O _{2y}	6807.8	Calcite	-0.31	-14.54	22	O _{1-2y}	6836.9	Calcite	2.12	-6.51
7	O _{2y}	6808.3	Calcite	-0.42	-14.71	23	O _{2y}	6772.4	Calcite	-0.52	-7.57
8	O _{2y}	6813.4	Calcite	-3.25	-13.08	24	O _{2y}	6726.8	Calcite	-0.78	-6.37
9	O _{1-2y}	6750.8	Calcite	1.59	-10.19	25	O _{2y}	6698.7	Calcite	-0.86	-6.91
10	O _{2y}	6749.3	Calcite	-2.01	-11.33	26	O _{2y}	6785.5	Calcite	0.12	-8.63
11	O _{2y}	6752.5	Calcite	0.06	-15.71	27	O _{1-2y}	6773.6	Calcite	0.27	-7.38
12	O _{2y}	6764.6	Calcite	-1.92	-9.25	28	O _{1-2y}	6836.9	Calcite	0.12	-6.34
13	O _{2y}	6723.2	Calcite	-1.63	-12.25	29	O _{1-2y}	6815.6	Bedrock	1.43	-4.14
14	O _{1-2y}	6694.1	Calcite	-4.09	-12.71	30	O _{1-2y}	6791.3	Bedrock	1.56	-6.04
15	O _{2y}	6712.5	Calcite	-1.34	-8.61	31	O _{2y}	6775.3	Bedrock	1.65	-7.16
16	O _{2y}	6756.2	Calcite	-0.59	-9.54	32	O _{2y}	6685.8	Bedrock	0.81	-5.17

Characteristics of inclusions

The greatest difference between the exposed environment and the burial diagenetic environment of carbonatite is the variations in the properties of the pore water (Goldstein 2001). Precipitation of cement indicates diagenesis of carbonatites, and the saline inclusions trapped within the cements have a close relationship with the diagenetic environment. The homogenization temperature serves as an important indicator for distinguishing diagenetic stages and fluid activity. The salinity varies with sedimentary environments; thus, the salinity of saline inclusions provides information on the chemical evolution of the diagenetic fluids (Li et al. 1996; Andrew et al. 2000; Lu and Shan 2015).

Previous studies have identified various types of inclusions, such as hydrocarbon and water inclusions. Hydrocarbon inclusions include single-phase gaseous hydrocarbon, single-phase liquid hydrocarbon, and two-phase gaseous and liquid hydrocarbon inclusions. Water inclusions include single-phase saline, two-phase gaseous and liquid saline, and three-phase hydrocarbon-containing saline inclusions. The influence of hydrocarbons on hydrocarbon inclusions or hydrocarbon-containing inclusions might result in estimation errors of temperature and salinity during the formation of the fillings. Therefore, this study attempts to discuss the diagenetic environment of the fillings using single-phase saline inclusions and two-phase gaseous and liquid saline inclusions (Table 2).

Physical characteristics of inclusions (Fig. 4a–i)

The shapes of the single-phase saline inclusions are generally round, square, oval, polygonal, or irregular. These

inclusions are distributed in groups in a belt-like pattern or evenly in calcites. However, some inclusions are accompanied by hydrocarbon inclusions distributed in a line or in a belt along cemented microfissures in calcites. A no-bubble state in single-phase liquid inclusions is a quasi-stable phenomenon that in most instances indicates low-trapping temperatures (Chi and Lu 2008; Zajacz et al. 2011). These inclusions appear to be transparent colorless or light brown in plane light without fluorescence. They have a general size of 3–40 μm with some reaching 85 μm . Single-phase saline inclusions account for more than 60% of all inclusions.

The shapes of the two-phase gaseous and liquid saline inclusions are generally round, polygonal, or rectangular; some are irregular in a few instances. These inclusions are distributed in groups in a belt-like pattern or evenly in calcites, although a few are accompanied by hydrocarbon inclusions and are distributed in a line or belt along the cemented microfissures in the calcites. These inclusions appear to be transparent, colorless, or light brown in plane light and have no fluorescence; their general size is 2–50 μm .

Chemical characteristics of two-phase gaseous and liquid saline inclusions

The salinity, freezing point, and homogenization temperature of the two-phase gaseous and liquid inclusions are shown in Table 2. The crossplot of salinity and homogenization temperature (Fig. 5) shows that the salinity of the inclusions in the Halahatang area varies greatly. The salt mass fraction of NaCl ranges from 0.53

Table 2 Results of two-phase gaseous and liquid inclusions

Sample no.	Depth/m	Stratum position	Sample	Gas–liquid ratio/vol%	Freezing point/ $^{\circ}\text{C}$	Homogenization Temperature/ $^{\circ}\text{C}$	$W_{\text{NaCl}}/\%$
1-1	6756.1	O _{2y} j	Calcite	5–10	–16.4 to –20.1	82–92	19.60–22.44
1-2	6756.1	O _{2y} j	Calcite	10–15	–3.9 to –7.5	95–119	6.30–11.10
2	6756.6	O _{2y} j	Calcite	5–10	–12.0 to –18.6	99–140	15.96–21.40
3	6733.1	O _{1–2y}	Calcite	5–10	–10.0 to –19.8	78–119	13.94–22.24
4	6574.7	O _{2y} j	Limestone	5–10	–0.3 to –1.1	80–129	0.53–1.74
5	6609.2	O _{2y} j	Calcite	5–10	–1.1 to –5.6	67–110	1.91–8.68
6	6807.8	O _{2y} j	Calcite	5–10	–6.8 to –18.0	72–128	10.24–20.97
7	6808.3	O _{2y} j	Calcite	5–10	–8.5 to –15.3	82–110	12.28–18.88
8	6813.4	O _{2y} j	Calcite	5–10	–1.5 to –5.6	69–110	2.57–8.68
9-1	6749.3	O _{2y} j	Calcite + fluorite	3–5	–1.9 to –4.5	59–83	3.23–7.17
9-2	6749.3	O _{2y} j	Calcite + fluorite	5–10	–11.2 to –14.9	92–122	15.17–18.55
10	6752.0	O _{2y} j	Calcite + fluorite	3–5	–2.7 to –11.8	73–95	4.49–15.76
11	6764.6	O _{2y} j	Calcite	3–5	–9.7 to –14.7	74–108	13.62–18.38
12	6823.0	O _{1–2y}	Calcite	3–5	–1.8 to –8.7	67–109	3.06–12.51
13	6694.0	O _{1–2y}	Calcite	3–5	–1.4 to –18.7	70–105	2.41–21.47

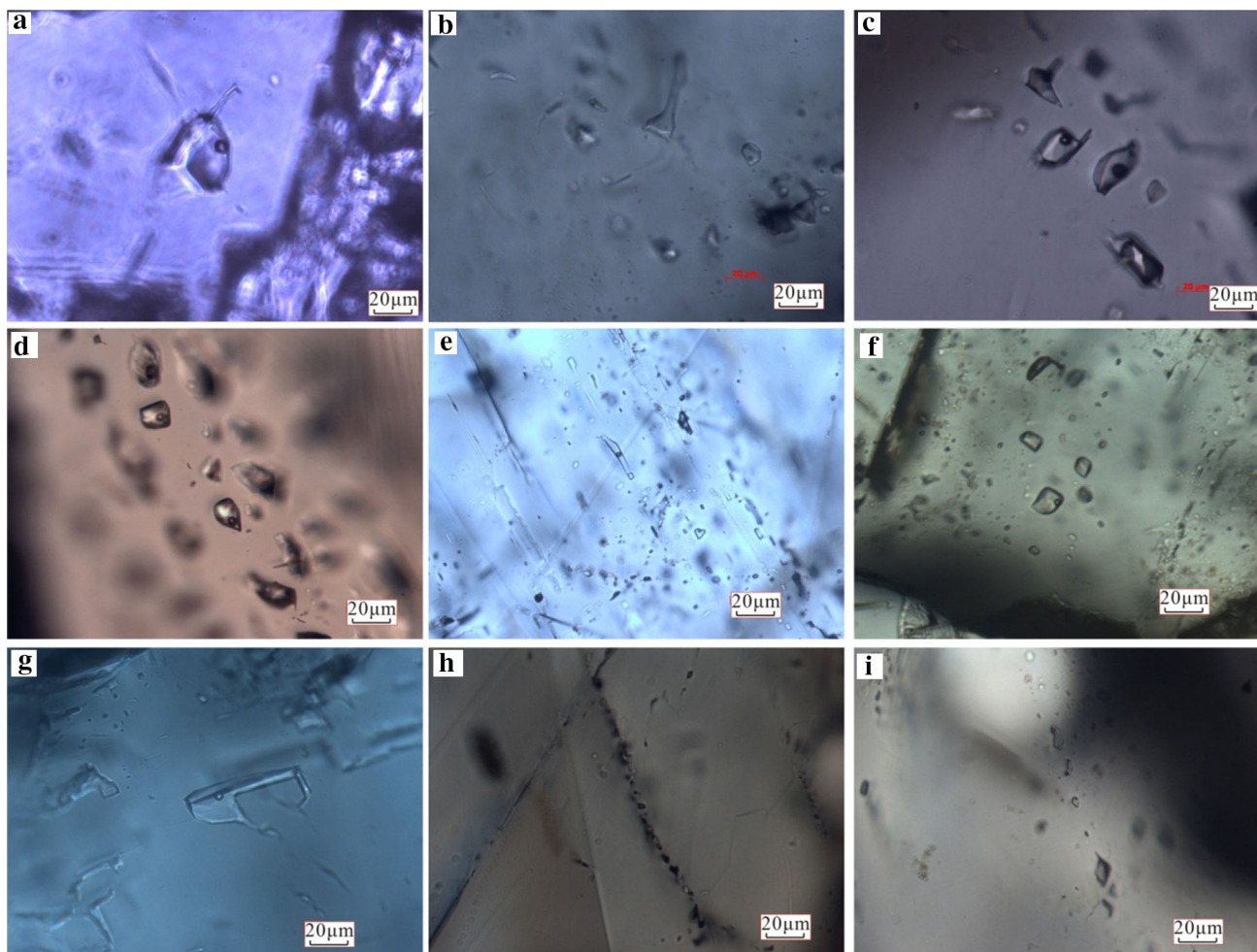


Fig. 4 Shapes and distribution characteristics of fluid inclusions in calcites. **a** Fluid inclusions distributed in small groups; *rice-shaped, polygon, irregular*; size 2–30 μm ; **b** fluid inclusions distributed in small groups; *rice-shaped, polygonal, rectangular, oval, irregular*; size 2–30 μm ; **c** fluid inclusions distributed throughout calcite, in small groups or in string of beads; *rice-shaped, oval, polygonal, and rectangular*; size 2–20 μm ; **d** fluid inclusions distributed throughout calcite, in small groups or in string of beads, with slight directionality; *rice-shaped, oval, polygon, and partly automorphic negative form*; size 2–25 μm ; **e** fluid inclusions distributed throughout calcite, in

groups or in lines; *rice-shaped, small rhombus, oval, polygonal, rectangular*; size 2–20 μm ; **f** fluid inclusions distributed throughout calcite, in groups or in lines; *rice-shaped, oval, polygonal and rhombic*; size 2–15 μm ; **g** fluid inclusions distributed throughout calcite or in small groups; *rice-shaped, rectangular, and polygonal*; size 2–40 μm ; **h** fluid inclusions distributed throughout calcite, in small groups or in lines; *rice-shaped, oval, polygonal and rectangular*; size 2–7 μm ; **i** fluid inclusions distributed throughout calcite, in small groups or in lines; *rice-shaped, oval, polygonal and rhombic*; size 1–10 μm

to 22.24%, indicating significant variations of karst fluid properties in this area. Overall, the inclusions in the Halahatang area can be divided into three types in terms of the salinity. Type I is low-salinity inclusion with a salinity mass fraction of NaCl ranging from 0.53 to 8.68%; this type is represented by samples 1-2, 4, 5, 8, 9-1, and 12. Type II is medium-salinity inclusion with a salt mass fraction of NaCl ranging from 8 to 18%; this type is represented by samples 7, 9-2, 10, 11, and 13. Type III is high-salinity inclusion with a salt mass fraction of NaCl ranging from 15 to 22.24%; this type is represented by Samples 1-1, 2, 3, and 6.

Discussion

Environmental and geological significance of carbon and oxygen isotopes

The $\delta^{18}\text{O}$ value of the bedrock and calcites filling the paleokarstic fissures and pores in the Halahatang area is generally negative, whereas the $\delta^{13}\text{C}$ values fluctuate over a broad range. This can be attributed to the meteoric water eluviation of $\delta^{12}\text{C}$ and to atmospheric CO_3^{2-} sources of $\delta^{16}\text{O}$ in an overall open environment resulting from the Ordovician uplift (Gasparrini et al. 2006; Azmy et al. 2009).

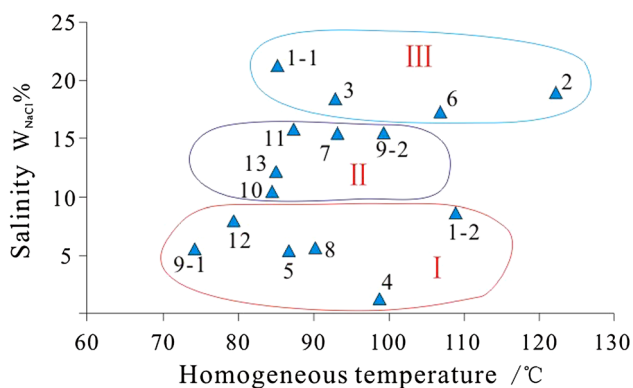


Fig. 5 Cross-diagram of salinity and homogenization temperature for inclusions

The crossplot of $\delta^{13}\text{C}$ – $\delta^{18}\text{O}$ (Fig. 6) indicates that the paleoenvironment can be categorized into four classes in terms of the calcites filling the karstic fissures and pores in the Halahatang Ordovician carbonatite (Table 3).

Class I is a marine environment during the syndiagenetic stage, which reflects the isotope characteristics of the early paleokarstification environment filling. $\delta^{13}\text{C}$ of the karst cave calcite ranges from 0.81 to 2.12‰, and $\delta^{18}\text{O}$ ranges from -7.16 to -4.14 ‰. The burial depth, temperature, leaching, and corrosion of the sediments can all affect $\delta^{13}\text{C}$ and $\delta^{18}\text{O}$ values. The $\delta^{13}\text{C}$ and $\delta^{18}\text{O}$ values increase with an increase in salinity, and $\delta^{18}\text{O}$ decreases with an increase in temperature. The $\delta^{18}\text{O}$ values tend to be more negative with increasing temperature and burial depth (McCaig

et al. 2000; Zhang et al. 2008). $\delta^{13}\text{C}$ is affected mostly by paleo-salinity and less by temperature, indicating the existence of a marine environment. The $\delta^{13}\text{C}$ values of limestone samples in this study are also within this range, suggesting a marine paleoenvironment.

Class II is weathered crust exposed in a karst freshwater environment. The $\delta^{13}\text{C}$ values in the filling calcite range from -4.09 to -3.12 , and the $\delta^{18}\text{O}$ values range from -15.17 to -10.25 ‰. Owing to the influence of atmospheric freshwater (Gasparrini et al. 2006), the $\delta^{13}\text{C}$ values, which were formed in an open environment, were apparently smaller than the bedrock carbon isotopic values. This environment lies above the water table; therefore, the corrosion-caused fissures and pores were filled with water and air, where water infiltrated and flowed only vertically. The $\delta^{18}\text{O}$ value of the diagenetic fabric is determined by temperature, isotopic composition of bedrock, and meteoric water rich in ^{12}C but poor in $\delta^{18}\text{O}$. Therefore, the $\delta^{13}\text{C}$ value drifted negatively, and $\delta^{18}\text{O}$ was strongly negative (Chen 1994; Shields et al. 2003).

Class III is a shallow-burial karst environment. The $\delta^{13}\text{C}$ values in the karst cave filling calcite are between -1.92 and -1.59 ‰, and the $\delta^{18}\text{O}$ values range from -10.19 to -6.34 ‰. $\delta^{18}\text{O}$ shows obvious negative bias, although $\delta^{13}\text{C}$ shows a slightly negative bias. Only one sample showed a positive $\delta^{13}\text{C}$ value (PDB) of 1.59‰, which might be attributed to the decomposition and methanation (CH_4) of organic matter caused by methane bacteria. The CH_4 formed from biochemical processes is rich in $\delta^{12}\text{C}$,

Fig. 6 Crossplot of carbon and oxygen isotopes for filling materials in the Ordovician karst cave system

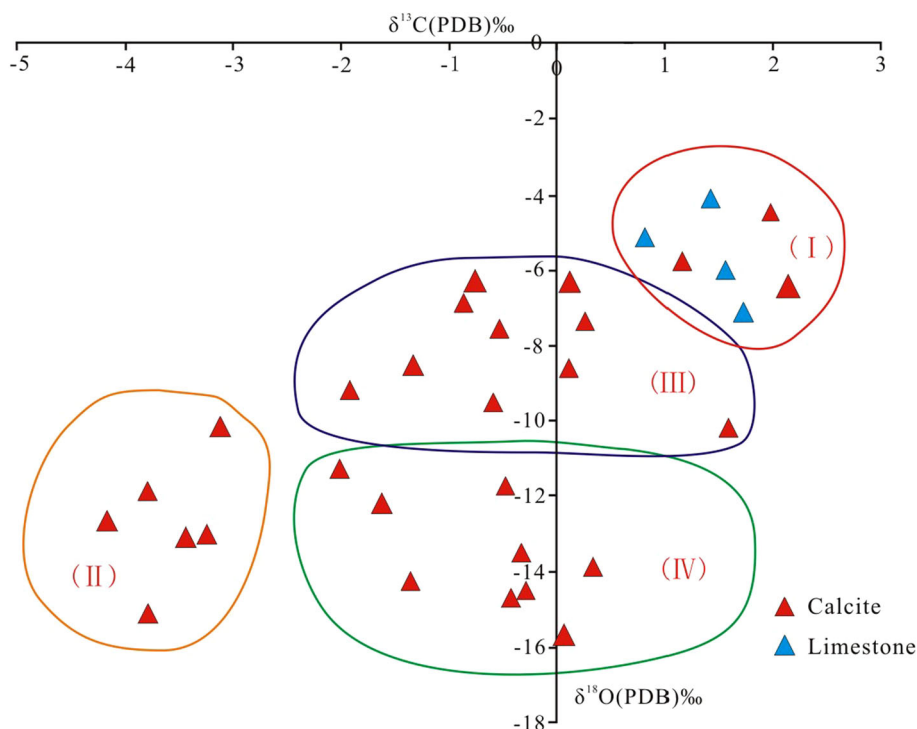


Table 3 Response characteristics of karst development stage and filling environment

Development period	Formation environment	Isotope features	
		$\delta^{13}\text{C}(\text{PDB})\text{‰}$	$\delta^{18}\text{O}(\text{PDB})\text{‰}$
I	Marine environment during syndiagenesis	0.81 to 2.12	−7.16 to −4.14
II	Atmospheric freshwater environment	−4.09 to −3.12	−15.17 to −10.25
III	Shallow-burial environment	−1.92 to 1.59	−10.19 to −6.34
IV	Deep-burial high-temperature environment	−2.01 to 0.34	−15.71 to −11.33

whereas the CO_2 has abundant $\delta^{13}\text{C}$. Because CO_2 released during the reaction of methane bacteria fermentation is rich in $\delta^{13}\text{C}$, the sedimentary filling has more positive values (Huang et al. 2008).

Class IV is a deep-burial high-temperature environment. $\delta^{13}\text{C}$ in calcite is between −2.01 and 0.34‰, and the $\delta^{18}\text{O}$ values range from −15.71 to −11.33‰. The $\delta^{18}\text{O}$ value shows a remarkably negative bias, reflecting a significant relationship between the formation of calcite filling and hydrothermal activity. Because of the influence of heat loss in the transformation of deep $\delta^{18}\text{O}$ in the burial stage (Lavoie and Chi 2006; Liu et al. 2012), the $\delta^{18}\text{O}$ values are significantly more negative than those of other classes.

Homogenization temperature and burial history analysis of the inclusions

A fluid inclusion is a closed micro-liquid or gaseous system trapped in mineral crystal. This fluid records information on the geological history of the rock and a relatively closed geochemical system; different periods of fluid inclusion filling in karst fissures and pores reflect different stages of mineralization (Nedkvite et al. 1993; Parnell et al. 2001).

The present study showed that the temperature of the two-phase gaseous and liquid saline inclusions is between 59 and 140 °C (Table 2). The Ordovician inclusions from different wells or from the same wells but at different depths showed different temperatures. For example, Inclusion 1-2 and Inclusion 2 from Sample 1 have maximum temperatures of 119 and 140 °C, respectively. Moreover, the gaseous and liquid inclusions from the same sample from the same well were different. For example, the homogenization temperatures of gaseous and liquid Inclusion 9-1 and Inclusion 9-2 from Sample 9 range from 59 to 83 °C and from 92 to 122 °C, respectively. These differences indicate that the Ordovician carbonatites in the Halahatang area experienced multi-stage diagenesis and modification at different temperatures.

The distribution frequency of the homogenization temperature divides the temperatures into three ranges of inclusion formation (Fig. 7). The first is 66–80 °C, during which time the greatest number of inclusions formed between 70 and 75 °C. The second is 81–95 °C, during which time the greatest number of inclusions formed

between 86 and 90 °C. The third is 96–120 °C, during which time fewer inclusions formed than those during the two prior divisions. However, in the temperature range of 96–120 °C, the number of inclusions increased dramatically in the temperature range of 101–105 and 116–120 °C, indicating the existence of a weak filling stage. In this study, only a few inclusions showed temperatures >120 °C, with a maximum temperature of 14 °C.

However, the maximum homogenization temperature of the two-phase gaseous and liquid saline inclusions in the Tahe oil field in the eastern Halahatang area can reach 200 °C (He et al. 2010; Li 2013), suggesting the possibility of abnormally high-temperature fluids in this area. However, these fluids exerted only very limited influence.

The formation of widely distributed single-phase liquid inclusions may be affected by a number of factors (Ford 1995; Xiao et al. 2002; Loucks et al. 2004). Abundant single-phase liquid inclusions are distributed throughout the calcites filling paleokarst fissures and pores in the study area. As a result, it is possible that a portion of the inclusions was formed in a low-temperature environment in which the temperature was lower than 50 °C. These low-temperature single-phase liquid inclusions resulted from exposure and paleokarstification of Ordovician carbonatites by meteoric water during the Caledonian.

The paleo-geothermal gradient of the study area is 25 °C/km, which is lower than the current gradient (Wang et al. 2013). Given a surface temperature of 15 °C, the temperatures of inclusion formation were calculated and projected onto a burial history map, as shown in Fig. 8. Four large-scale paleokarstification events and filling periods were identified, including karstification by meteoric water during the Caledonian, burial karstification during the late Hercynian, burial karstification during the Indosinian–Yanshanian, and burial karstification during the Himalayan. These events are consistent with the carbon and oxygen isotopic results of the present study.

Conclusions

The Ordovician carbonatites in the Halahatang area experienced three depositional hiatuses, i.e., pinching out of the strata from south to north, development of pure and thick

Fig. 7 Distribution of homogenization temperature for two-phase saline inclusions

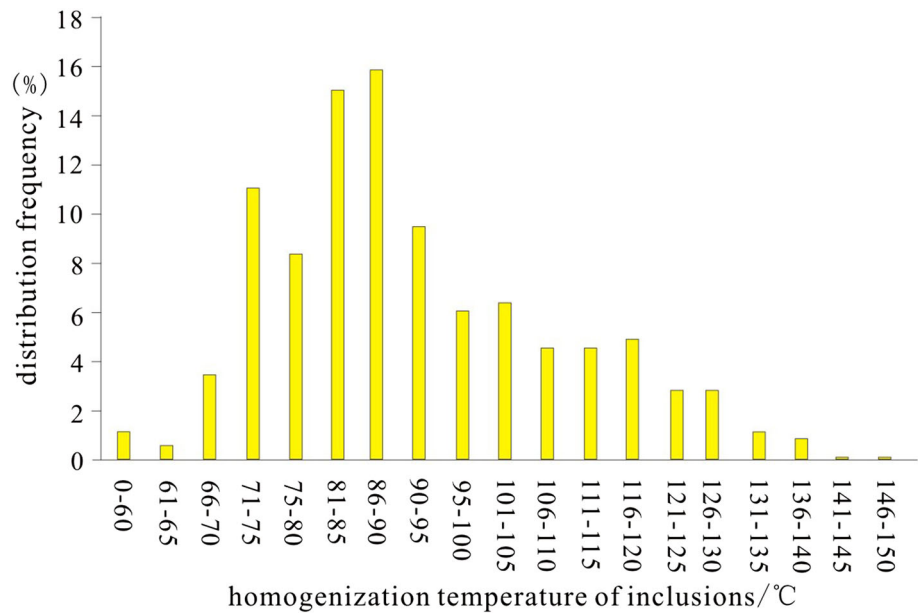
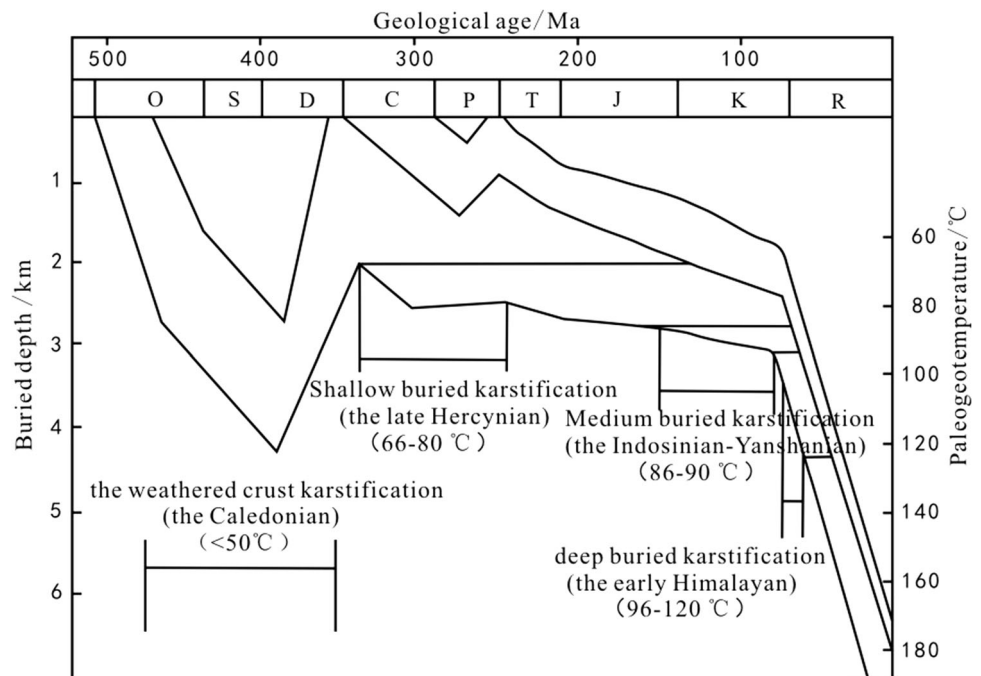


Fig. 8 Filling history for filled calcite in the Ordovician karst cave system in the Halahatang area



limestone in the Yijianfang and Yingshan formations, and development of paleokarst. The carbon and oxygen isotopic analysis shows that the $\delta^{13}\text{C}$ value varies widely from 2.12 to -4.09% , with an average of -0.65% ; however, the $\delta^{18}\text{O}$ values show obvious negative bias, ranging from -4.14 to -15.71% with an average of -9.95% . These results indicate four classes of paleoenvironment of carbonatite karstification: a syndiagenetic marine environment, weathered crust exposed in a karst freshwater environment, a shallow-burial karst environment, and a deep-burial high-temperature environment.

The saline inclusions of calcites in the fissures and pores of the Ordovician carbonatite paleokarst can be divided into three types: low-salinity, medium-salinity, and high-salinity inclusions. Analysis of homogenization temperature indicates that the inclusions were formed mainly in three temperature ranges. These results are consistent with the carbon and oxygen isotopes and reveal four large-scale paleokarstification events and filling periods with burial karstification during the late Hercynian, the Indosinian-Yanshanian, and the Himalaya in addition to karstification by meteoric water during the Caledonian.

Acknowledgements This research was funded by the National Natural Science Foundation Project (41302122), National Key Basic Research Development (973 Program) Project (2011CB201001), and Public Welfare Industry Scientific Special Research (201211082) in Ministry of Land and Resources (MLR). The authors express sincere thanks to the reviewers and editors who offered valuable advice to improve this paper.

References

- Andrew C, Aplin A, Steve R (2000) Confocal microscopy of fluid inclusions reveals fluid-pressure histories of sediments and an unexpected origin of gas condensate. *Geology* 28:1047–1050
- Azmy K, Knight I, Lavoie D, Chi G (2009) Origin of dolomites in the Boat Harbour Formation, St. George Group, in western Newfoundland, Canada: implications for porosity development. *B Can Pet Geol* 57:81–104
- Burley SD, Mullis J, Matter A (1989) Timing diagenesis in the Tartan reservoir (UK North Sea): constraints from combined cathodoluminescence microscopy and fluid inclusion studies. *Mar Pet Geol* 6:98–120
- Chen RK (1994) Application of stable oxygen and carbon isotope in the research of carbonate diagenetic environment. *Acta Sedimentol Sin* 12:11–21 **(in Chinese with English abstract)**
- Chen JS, Li Z, Wang ZY, Tan XC, Li L, Ma Q (2007) Paleokarstification and reservoir distribution of Ordovician carbonates in Tarim Basin. *Acta Sedimentol Sin* 25:858–868 **(in Chinese with English abstract)**
- Chi GX, Lu HZ (2008) Validation and representation of fluid inclusion microthermometric data using the fluid inclusion assemblage (FIA) concept. *Acta Pet Sin* 24:1945–1953 **(in Chinese)**
- Feng JL, Cao J, Hu K, Peng XQ, Chen Y, Wang YF, Wang M (2013) Dissolution and its impacts on reservoir formation in moderately to deep buried strata of mixed siliciclastic carbonate sediments, northwestern Qaidam basin, Northwest China. *Mar Pet Geol* 39:124–137 **(in Chinese with English abstract)**
- Ford DC (1995) Paleokarst as a target for modern karstification. *Carbonates Evaporites* 10:138–147
- Gasparini M, Bechstaedt T, Boni M (2006) Massive hydrothermal dolomites in the south western Cantabrian Zone (Spain) and their relation to the Late Variscan evolution. *Mar Pet Geol* 23:543–568
- Goldstein RH (2001) Fluid inclusions in sedimentary and diagenetic systems. *Lithos* 55:159–193
- Gu JY (2000) Characteristics and origin analysis of dolomite in lower Ordovician of Tarim Basin. *XJ Pet Geol* 21:120–122 **(in Chinese)**
- Haszeldine RS, Samson IM, Cornfort C (1984) Dating diagenesis in a petroleum basin, a new fluid inclusion method. *Nature* 307:354–357
- He ZL, Peng ST, Zhang T (2010) Controlling factors and genetic pattern of the Ordovician reservoirs in the Tahe area, Tarim Basin. *Oil Gas Geol* 31:743–752
- Huang SJ, Qing HR, Huang PP, Hu ZW, Wang QD, Zou ML, Liu HN (2008) Evolution of strontium isotopic composition of seawater from Late Permian to Early Triassic based on study of marine carbonates, Zhongliang Mountain, Chongqing, China. *Sci China Ser D* 51:528–539 **(in Chinese)**
- Jia ZY, Cai ZX (2004) Carbonate paleo-weathered crust reservoirs (body). *Geol Sci Technol Inf* 23:94–104 **(in Chinese with English abstract)**
- Jin ZJ, Cai LG (2006) Exploration prospects, problems and strategies of marine oil and gas in China. *Oil Gas Geol* 27:722–730 **(in Chinese with English abstract)**
- Lavoie D, Chi GX (2006) Hydrothermal dolomitization in the Lower Silurian La Vieille Formation in northern New Brunswick: geological context and significance for hydrocarbon exploration. *B Can Pet Geol* 54:380–395
- Li Y (2013) The theory and method for development of carbonate fractured-cavity reservoirs in Tahe oilfield. *Acta Pet Sin* 34:115–121
- Li D, Liang D, Jia C (1996) Hydrocarbons accumulations in the Tarim Basin, China. *AAPG Bull* 80:1587–1603
- Liu GD (2007) Suggestions on secondary pioneering of Chinese oil and gas resources. *Spec Oil Gas Reserv* 14:1–4 **(in Chinese with English abstract)**
- Liu XP, Wu XS, Zhang XZ (2004) Geochemistry characteristics of carbon and oxygen isotopes of Ordovician carbonate palaeokarst reservoir in the western region of Lungu, Tarim Basin. *J Xi An Shi you University Nat Sci Ed* 19:69–72 **(in Chinese with English abstract)**
- Liu CG, Li GR, Zhu CL, Liu GY (2008) Geochemistry characteristics of carbon, oxygen and strontium isotopes of calcites filled in karstic fissure-cave in Lower–Middle Ordovician of Tahe Oilfield, Tarim Basin. *Earth Sci J China Univ Geosci* 33:377–386 **(in Chinese)**
- Liu JQ, Li Z, Huang JC (2012) Distinct sedimentary environments and their influences on carbonate reservoir evolution of the Lianglitag formation in the Tarim basin, Northwest China. *Sci China Earth Sci* 42:1802–1816
- Liu KY, Bourdet J, Zhang BS (2013) Hydrocarbon charge history of the Tazhong Ordovician reservoirs, Tarim Basin as revealed from an integrated fluid inclusion study. *Pet Explor Dev* 40:171–180 **(in Chinese)**
- Liu XW, Zhu YF, Su J, Wang K, Zhang BT (2014) The characteristics and the controlling accumulation factors of buried hill reservoir in Halahatang, Tarim Basin. *Journal South West Pet Univ Sci Technol Ed* 36:37–46 **(in Chinese with English abstract)**
- Loucks RG, Mescher PK, McMechan GA (2004) Three-dimensional architecture of a coalesced collapsed-paleocave system in the Lower Ordovician Ellenburger Group Central Texas. *AAPG Bull* 88:545–564
- Lu HZ, Shan Q (2015) Composition of ore forming fluids in metal deposits and fluid inclusion. *Acta Pet Sin* 31:1108–1116
- Mafia B (1986) The Permo-Triassic vein and paleokarst ores in southwest Sardinia: contribution of fluid inclusion studies to their genesis and paleoenvironment. *Miner Depos* 21:53–62
- Murray RC (1957) Hydrocarbon fluid inclusions in quartz. *AAPG Bull* 41:950–952
- McCaig AM, Tritlla J, Banks DA (2000) Fluid mixing and recycling during Pyrenean thrusting: evidence from fluid inclusion halogen ratios. *Geochim Cosmochim Acta* 64:3395–3412
- Munz IA (2001) Petroleum inclusions in sedimentary basins: systematics, analytical methods and applications. *Lithos* 55:195–211
- Nedkvite T, Karlsen DA, Bjorlykke K (1993) Relationship between reservoir diagenetic evolution and petroleum emplacement in the Ula Field, North Sea. *Mar Pet Geol* 10:225–270
- Ni XF, Zhang LJ, Shen AJ, Pan WQ, Qiao ZF (2009) Paleokarstification types, karstification periods and superimposition relationship of Ordovician carbonates in northern Tarim Basin. *Geol China* 36:1312–1321 **(in Chinese with English abstract)**
- Ni XF, Zhang LJ, Shen AJ, Qiao ZF, Han LJ (2010) Diagenesis and pore evolution of the Ordovician karst reservoir in Yingmaili-Halahatang region of Tarim Basin. *J Palaeogeogr* 12:101–113 **(in Chinese with English abstract)**
- Osborne M, Haszeldine S (1993) Evidence for resetting of fluid inclusion temperatures from quartz cements in oilfields. *Mar Pet Geol* 10:271–278

- Pagel M, Poty B (1983) The evolution of composition, temperature and pressure of sedimentary fluids over time: a fluid inclusion reconstruction. In: Durand B (ed) *Thermal phenomena in sedimentary basins*. Gulf Publishing Company, Houston, pp 71–88
- Pagel M, Walgenwitz F, Dubessy J (1985) Fluid inclusions in oil and gas-bearing sedimentary formations. In: Bunnuss J (ed) *Thermal modeling in sedimentary basins*. Gulf Publishing Company, Houston, pp 565–583
- Parnell J, Middleton D, Chen HH (2001) The use of integrated fluid inclusion studies in constraining oil charge history and reservoir compartmentation: example from the Jeanne d'Arc basin, offshore Newfoundland. *Mar Pet Geol* 18:535–549
- Roedder E (1979) Fluid inclusion evidence on the environments of sedimentary diagenesis. *SEPM Spec Publ* 26:89–107
- Shields GA, Carden GAF, Veizer J (2003) Sr, C and O isotope geochemistry of Ordovician brachiopods: a major isotopic event around the Middle-Late Ordovician transition. *Geochim Cosmochim Acta* 67:2005–2025
- Su ZT, Chen HD, Lin LB, Zhao JX, Xu Q (2010) Character of palaeokarst and its reservoirs significance of Ordovician Tabamiaoarea, Ordos. *Xinjiang Geol* 28:180–185 **(in Chinese with English abstract)**
- Veizer J, Ala D, Azmy K, Bruckschen P, Buhl D, Bruhn F, Diener A, Ebnet S, Godderis Y, Jasper T, Korte C, Pawellek F, Podlaha OG, Strauss H (1999) $^{87}\text{Sr}/^{86}\text{Sr}$, ^{13}C and ^{18}O evolution of Phanerozoic seawater. *Chem Geol* 161:58–88
- Wang BQ, Al-Aasm IS (2002) Karst-controlled diagenesis and reservoir development: example from the Ordovician main-reservoir carbonate rocks. *AAPG Bull* 86:1639–1658
- Wang ZM, Zang N, Lu YH, Fang QF, Chen RY, Zhang BS, Ju FP (2013) Study of hydrocarbon inclusions of Ordovician in Halahatang-Yingmaili Area, Tarim Basin. *Xinjiang Pet Geol* 34:103–105 **(in Chinese with English abstract)**
- Wen HG, Chen HR, Wen LB, Zhou G, Feng QP, Li S (2014) Diagenetic fluids of paleokarst reservoirs in Carboniferous from eastern Sichuan Basin: some evidence from fluid inclusion, trace element and C-O-Sr isotope. *Acta Pet Sin* 30:655–666 **(in Chinese)**
- Wu GH, Li HH, Zhang LP, Wang CL, Zhou B (2012) Reservoir forming conditions of the Ordovician weathering crust in the Maigaiti slope, Tarim basin, NW China. *Pet Explor Dev* 39:144–153 **(in Chinese with English abstract)**
- Xia MJ, Dai JX, Zou CN, Wang ZC, Tao SZ (2007) Caledonian karst palaeogeomorphology and the forming condition of gas pool, southern Ordos basin. *Pet Explor Dev* 34:291–298 **(in Chinese with English abstract)**
- Xiao XM, Liu ZF, Liu DH (2002) Applications of fluid inclusions in the reservoir to the studies of gas pool forming time. *Chin Sci Bull* 47:957–960
- Yan ZB, Guo FS, Pan JY (2005) Application of C, O and Sr isotope composition of carbonates in the research of paleoclimate and paleoceanic environment. *Contrib Geol Miner Resour Res* 20:54–55
- Zajacz Z, Seo JH, Candela PA, Piccoli PM, Tossell JA (2011) The solubility of copper in high-temperature magmatic vapors: a quest for the significance of various chloride and sulfide complexes. *Geochim Cosmochim Acta* 75:2811–2827
- Zhang K, Wang DR, Bryan GH (2004) Reservoir characterization of the Ordovician oil and gas pools in the Tahe oilfield, Tarim basin, Northwest China. *Pet Explor Dev* 31:123–126 **(in Chinese)**
- Zhang C, Yu BS, Fan TL, Hang WH, Zhu JQ, Wu SQ (2008) The characteristics of cave fillings of carbonates in the Lower Ordovician and their diagenetic environments in northern Tarim basin. *Earth Sci Front* 15:100–108 **(in Chinese with English abstract)**
- Zhang B, Zheng RC, Wang XB, Luo Y, Li W, Wen HG, Hu ZG (2011) Paleokarst and reservoirs of the Huanglong Formation in eastern Sichuan Basin. *Pet Explor Dev* 38:257–267 **(in Chinese with English abstract)**
- Zhang XF, Li M, Chen ZY, Jiang H, Tang JW, Liu B, Gao JX, He YL (2012) Characteristics and karstification of the Ordovician carbonate reservoir, Halahatang area, northern Tarim Basin. *Acta Pet Sin* 28:815–826 **(in Chinese with English abstract)**
- Zhang QY, Liang B, Cao JW, Dan Y, Li JR (2014) Palaeogeomorphology and karst development conditions of Yijianfang Formation in Hanilcatam Area. *Fault Block Oil Gas Field* 21:413–415 **(in Chinese with English abstract)**
- Zhang QY, Liang B, Cao JW, Yong Dan, Li SY, Li JR, Hao YZ (2015) Research of geochemistry characteristics of carbon and oxygen isotopes of Ordovician Palaeokarst Reservoir in the East of Lungu-7, North Tarim Basin. *Geol Sci Technol Inf* 34:52–56 **(in Chinese)**
- Zheng YF, Chen JF (2000) *Stable Isotope Geochemistry*. Science Press, Beijing, pp 143–217 **(in Chinese)**
- Zhu GY, Zhang SC, Liang YB (2005) Isotopic evidence of TSR origin for natural gas bearing high H_2S contents within the Feixianguan Formation of the northeastern Sichuan Basin, southwestern China. *Sci China* 48:1960–1971